



HAL
open science

Numerical prediction of sediment deposition at a river confluence using an euler-lagrange method

Souria Hamidouche, Boris Arcen, Anne Tanière

► **To cite this version:**

Souria Hamidouche, Boris Arcen, Anne Tanière. Numerical prediction of sediment deposition at a river confluence using an euler-lagrange method. 9th International Conference on Multiphase Flow, May 2016, Firenze, Italy. hal-03154039

HAL Id: hal-03154039

<https://hal.univ-lorraine.fr/hal-03154039>

Submitted on 26 Feb 2021

HAL is a multi-disciplinary open access archive for the deposit and dissemination of scientific research documents, whether they are published or not. The documents may come from teaching and research institutions in France or abroad, or from public or private research centers.

L'archive ouverte pluridisciplinaire **HAL**, est destinée au dépôt et à la diffusion de documents scientifiques de niveau recherche, publiés ou non, émanant des établissements d'enseignement et de recherche français ou étrangers, des laboratoires publics ou privés.

Numerical prediction of sediment deposition at a river confluence using an Euler-Lagrange method

Souria Hamidouche¹, Boris Arcen² and Anne Tanière¹

¹Université de Lorraine, LEMTA, UMR 7563,

Vandoeuvre-lès-Nancy, F-54500, France

Souria.hamidouche@univ-lorraine.fr

² Université de Lorraine, LRGP, UMR 7274,
Nancy, F-54001, France

Abstract

Sediment deposition near to a river confluence is a crucial challenge for navigation since it can strongly affect the bed morphology and thus the barges traffic. The prediction of particle deposition is thus important in order to optimize the dredging operations which are necessary to maintain a sufficient draft. In the present study, we numerically examine the transport and deposition process of sediments at Scarpe and Escaut confluence (north of France) using an Euler-Lagrange approach. This method is known to be able to accurately predict the behaviour and spatial distribution of inertial particles in turbulent fluid flow. Nonetheless, contrary to the standard method (based on convection-diffusion equation for sediment concentration) usually used to predict the behaviour of sediments in such a complex configuration, it has a higher computational cost. In our study, the mean fluid flow is predicted by solving the 3D Reynolds-Averaged Navier-Stokes (RANS) equations. The trajectory of each sediment is then computed from the particle equation of motion with a stochastic dispersion model which predicts the sediment/turbulence interaction.

Keywords : natural confluence, sediment deposition, bed discordance, euler-lagrange method, dispersion model

1. Introduction

Spatial distribution of sediment particles deposition in a confluence is an important aspect for the navigation of barges. Therefore, to ensure an appropriate depth for the navigation, it requires an expensive maintenance dredging. The need of controlling and optimising the dredging operations has motivated this study of particle deposition modelling within a natural bed confluence. A better understanding of the flow patterns, sediment deposition and bed evolution is necessary to keep the navigation of barges. However, sediment deposition in confluences is governed by a complex interaction between the convergence of incoming flows and bed morphology. This complexity of flow patterns was firstly studied experimentally by Taylor [1] and was pursued in other studies [2, 3, 4, 5]. The analysis of bed morphology evolution was carried out experimentally with a movable bed by [6, 7, 4, 8]. Field investigations were performed at river confluences primarily to study the major features of mean and turbulent structures of the flow and secondly to evaluate the relevance of experimental and numerical models on flow patterns and bed morphology under natural conditions [9, 10, 11]. Although these field studies provided valuable insight of flow patterns for particular river conditions, they did not give pertinent parameters which control the nature of flow structures and the three-dimensional development of the incoming streams. Numerical modelling provides an alternative method to examine confluence characteristic since a detailed description of 3D patterns of the flow can be done, both for confluences with an artificial bed [5, 12] and confluences with a natural bed [13, 14,15]. However, modelling particles dispersion or deposition in an artificial or natural river confluence remains undone.

Previous experimental studies used for predicting the sediment deposition in rivers were mainly based on empirical criteria [16, 17, 18] involving the settling particle velocity and bed shear

stress. In other studies, authors deduced the particle deposition only on the analyses of the carrier fluid flow velocities. Indeed, authors treated sediment as particle without inertia (passive scalar), the particle deposition is then predicted only through the study of the characteristics of the carrier fluid flow as the mean longitudinal and wall-normal velocities, *rms* of velocities, etc.) [3, 10]. Recently, nonintrusive image technics were used to obtain instantaneous measures of fluid flow and particles velocities in order to better understand the particle/fluid interaction [19]. The present study will complement previous ones since the purpose of this paper is to provide a numerical investigation on the particle deposition process at a river confluence using an Euler-Lagrange approach which seems original since only few studies were dedicated particle deposition in rivers [21]. Moreover, no study exists for the case of the confluence zone. This Lagrangian method was largely used to predict the deposition of aerosol particles [20].

In the present study, the carrier phase is calculated by using a 3D RANS approach whereas the second Newton law is used to predict the instantaneous motion of particles. However, only mean fluid flow is predicted with RANS approach whereas the particle equation of motion necessitates instantaneous fluid velocity information which has to be known at the particle location. A dispersion model is thus necessary, i.e. the fluctuating fluid velocity at the particle location must be predicted. As a first approximation, an eddy interaction model (EIM), available on *Ansys Fluent* code, will be used to generate such randomly fluctuating velocities of the fluid at particle position. The particle/turbulence interactions can be then better modelled since through the resolution of the particle equation, the spatial distribution of particle can be deduced. From the results, we will be able to analyse the effect of the gravity and of the particle /turbulence interactions on particle deposition. A one way coupling assumption is adopted in the present work.

2. Study site

The study area is the confluence of Scarpe and Escaut which is located at Mortagne-du-Nord in France. The confluence has a symmetric planform (*Y-shape*) with a discordant bed. The two incoming channels join the post-confluence at an angle of about 37-39° (Fig. 1). Bathymetric data revealed the existence of a point bar at the upstream of the junction corner (see dashed black line in Fig. 1).

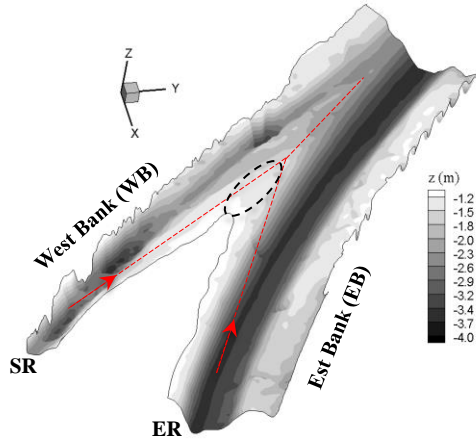


Figure 1 Confluence between the Scarpe River (SR) and Escaut River (ER). Contours show the confluence bathymetry (the free surface corresponds to $z = 0$ m).

3. Simulation procedure

3.1. A 3D RANS simulation

The flow of the natural bed confluence is modelling through the use of 3D Reynolds-Averaged Navier-Stokes simulations (RANS). The mean fluid flow is solved using RANS equation using the commercial software *Ansys Fluent* in Ref. [22]. This system involves the continuity equations Eqn (1) and the momentum equation Eqn (2).

$$\frac{\partial \rho_f \bar{u}_i}{\partial x_i} = 0, \quad (1)$$

$$\frac{\partial \rho_f \bar{u}_i}{\partial t} + \frac{\partial \rho_f \bar{u}_i \bar{u}_j}{\partial x_j} = -\frac{\partial \bar{p}}{\partial x_i} + \frac{\partial}{\partial x_j} \left[\mu \left(\frac{\partial \bar{u}_i}{\partial x_j} + \frac{\partial \bar{u}_j}{\partial x_i} \right) \right] + \frac{\partial}{\partial x_j} \left(-\rho_f \overline{u'_i u'_j} \right), \quad (2)$$

where, \bar{u}_i ($i = 1, 2, 3$) are mean velocities, x_i are coordinates, ρ_f is the water density, μ is the dynamic viscosity, \bar{p} is the mean pressure and $\overline{u'_i u'_j}$ is the Reynolds stresses which must be closed. The Reynolds stresses $\overline{u'_i u'_j}$ in Eqn. 2 cannot be calculated directly and required additional models. Two model families are chosen, the $k-\varepsilon$ and the $k-\omega$ which necessitate to solve two supplementary equations. In the $k-\varepsilon$ family, the

Renormalization Group (RNG) $k-\varepsilon$ turbulence model coupled with *Standard Wall Functions* is used in Ref. [23]. This modified version is better suited in flows with significant mean strain as is the case in confluences Ref. [13]. For the second one, the $k-\omega$ SST (Shear Stress Transport) model is adopted which is a combination of $k-\varepsilon$ and $k-\omega$ models model (Menter, 1994). In this model, a $k-\omega$ model is used in the inner boundary layer whereas a $k-\varepsilon$ model is used in the outer region of the boundary layer as well as outside of it Ref. [24]. For more details, refer to *Ansys Fluent* code in Ref. [22].

A finite volume method is used to discretize the incompressible Navier–Stokes equations with steady state flow conditions. Coupling of velocity and pressure is achieved using the Semi-Implicit Method for Pressure-Linked Equations (SIMPLE) algorithm. The computational domain was meshed with about 4 million cells. Natural conditions of the river confluence correspond to the conditions at the site during the year 2010, issued from field measurements (*Voies Navigables de France*). As initial conditions for inflow sections (ER and SR) the mean mass flow rate released are 19.93 m³/s and 5.16 m³/s, respectively (See Fig. 1). The channel bed and lateral walls are treated as rough no-slip boundaries, while a symmetry condition is adopted for the free surface.

3.2. Particle trajectories

The present simulation deals with spherical, solid particles smaller than the smallest Kolmogorov length scale and with low density ratio ($\rho_f / \rho_p < 1$, where subscription f and p denote fluid and particle, respectively). Consequently, under these assumptions and taking into account the effects of gravitational acceleration and drag forces, the particle of motion can be reduced to :

$$\frac{d\vec{u}_p}{dt} = -\frac{1}{\tau_p} (\vec{u}_p - \vec{u}_f) + \frac{(\rho_p - \rho_f) \vec{g}}{\rho_p}, \quad (3)$$

where \vec{u}_p is the velocity of the particle with density ρ_p . \vec{u}_f is the fluid velocity at the particle location. \vec{g} is the gravitational acceleration. τ_p is the particle relaxation time which is defined as :

$$\tau_p = \frac{\rho_p}{\rho_f} \frac{4d_p}{3C_D \|\vec{u}_p - \vec{u}_f\|}, \quad (4)$$

where d_p is particle diameter and C_D is the drag coefficient which depends on the flow regime. The expression of C_D is given by Ref. [25] as follow :

$$C_D = \frac{K_1}{\text{Re}_p} + \frac{K_2}{\text{Re}_p^2} + K_3. \quad (5)$$

Here, the empirical constants K_1 , K_2 and K_3 depend on the particles Reynolds number and are detailed in Ref. [25]. The use of a particle Lagrangian tracking necessitates to generate the fluid velocity fluctuation at particle location. This can be done through the use of a stochastic dispersion model, which is by default in *Ansys fluent* code, an eddy interaction model (EIM) developed by Ref. [26]. The EIM is based on the concept of energy containing turbulent eddies, where turbulent dispersion

of particles is modelled as a succession of interaction between these eddies and particles. The turbulent eddies are represented by instantaneous properties consisting of mean and fluctuating quantities. The RANS equations provide the averaged quantity and the fluctuating quantity are assumed to be isotropic and are selected randomly from a Gaussian probability distribution, whose standard deviation (σ_{ii}) is related to the turbulent kinetic energy (k) as follow :

$$\sigma_{ii} = \sqrt{u'^2} = \sqrt{v'^2} = \sqrt{w'^2} = \sqrt{\frac{2k}{3}}. \tag{6}$$

For particle trajectories calculation, a fifth-order Runge-Kutta method developed by Ref. [27] is used. The total number of particles injected, with a diameter of $19.99 \mu m$, in both ER and SR simultaneously is 10382 and their initial velocity is the same as the surrounding fluid. Every particle is tracked till it crosses the outlet boundary condition or hits the bed confluence, where a trap boundary condition is set. The maximum time steps to track every particle are fixed to 50,000,000, which was assumed to be sufficient for the slowest moving particles to have passed through the domain. However, these time steps are variable and the total traveling time is different per particle, therefore.

4. Results and discussions

Confluence morphology is governed by bed planform (i.e., discordance) and the momentum flux ratio (Mr) between the two incoming flows [10]. This latter is calculated for local conditions site as :

$$Mr = \frac{\rho_f Q_{v_{SR}} V_{SR}}{\rho_f Q_{v_{ER}} V_{ER}}, \tag{7}$$

where, Q_v is discharge (m^3/s) and V is cross-sectional mean velocity (m/s). Since the momentum ratio between the incoming rivers is about 0.23, a great influence in hydrodynamic conditions is supposed to occur on discordance bed confluence. As a consequence, the penetration of ER into SR is increased Ref. [11].

4.1. Flow characteristic at river confluence

The presence of a point bar at the upstream of the corner junction (Fig. 1) induces a decrease in the strength of the flow and minimizes the penetration of ER into SR. Results from Figure 2 shows clearly the development of a stagnation zone near the upstream of the junction corner, between section A and section B, where values of velocity magnitude are small. This zone extends into the tributary channel (SR), as it is observed by Ref. [11]. A region of low velocity magnitude is also observed along the west bank. It can be seen, that these trends are observed whatever the models used (*RNG k-ε* and *k-ω SST* in Fig. 2). Figure 3 presents a zoom at the junction, where a recirculation zone is created upstream the junction. This zone is characterised by the presence of vortices.

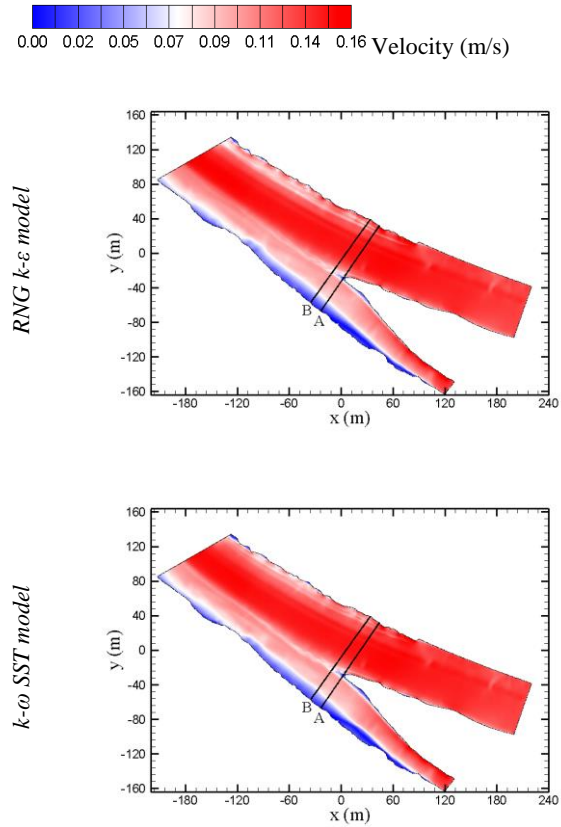


Figure 2 Velocity magnitude contours at $z = -0.5$ m for RANS simulations.

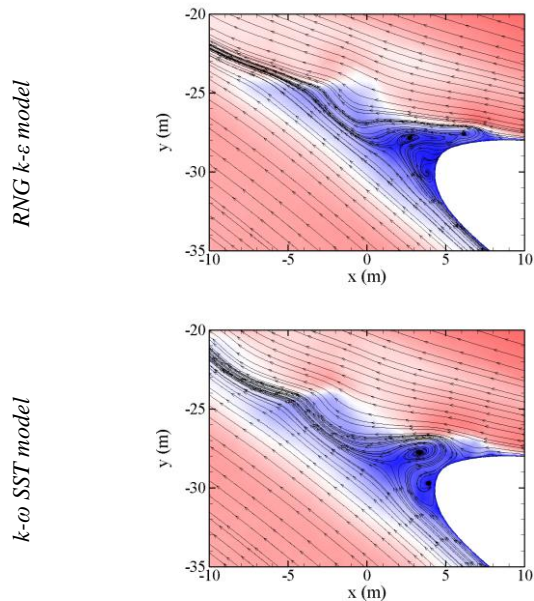


Figure 3 Zoom at the junction. Velocity magnitude contours at $z = -0.5$ m for RANS simulations.

A sharp difference is noticed in simulations performed by the *RNG k-ε* model and *k-ω SST* model, where predictions of the stagnation zone show that this zone is longer with *k-ω SST* than with *RNG k-ε* model. More details seem to be obtained when *k-ω SST* model is used.

4.2. Analysis of the mixing layer

The convergence of two no-parallel flows of unequal velocities creates a zone of shear, commonly called: zone of mixing layer. According to the literature, the position of this zone depends on the value of Mr (Ref. [10]), the angle between the two incoming streams (Ref. [29]) and the change in bathymetry (i.e., bed discordance) [3, 10]. In the mixing zone and with the presence of bed discordance, a lateral motion of the flow from the deeper channel (ER) towards the shallower channel, enhances this zone and causes the distortion of this latter [28, 3]. In addition, when $Mr < 1$, the mixing interface shifts to the tributary channel (SR), and this lateral distortion is illustrated by the orientation of high values of k observed in section A and B (Fig. 4 and Fig. 5), trends which have been observed in previous studies [28, 3, 10].

Near the junction (section A), the shear layer is characterized by a high level of turbulence [28, 3, 14, 30]. Moreover, within this mixing layer, regions of reduced velocities correspond to the highest level of k . According to previous studies [30], this shear layer is tridimensional, since it develops both vertically and laterally (Fig. 4 and Fig. 5). According to the results, the mixing layer is present whatever the models used ($RNG\ k-\epsilon$ and $k-\omega\ SST$). However, the prediction of the intensity values of k is different. For the $k-\omega\ SST$ model, highest levels of k are found in section A, where the maximum value is about $2\text{ cm}^2/\text{s}^2$ (near the junction corner), while it is about $0.7\text{ cm}^2/\text{s}^2$ in section B. Regarding the $RNG\ k-\epsilon$ model at section A, the highest value is only $0.8\text{ cm}^2/\text{s}^2$ and is about $0.4\text{ cm}^2/\text{s}^2$ for the section B.

In this study, neither a separation zone nor helical cells are observed within the confluence, as it is predicted and presented by Ref. [7]. According to the experimental study performed by Ref. [4], it was found that the flow separation occurs only at 90° angle for symmetrical confluences. As a consequence, the absence of the flow separation can result either or both from:

- the presence of depositional bar at the junction corner;
- the presence of bed discordance.

In addition, these models ($RNG\ k-\epsilon$ and $k-\omega\ SST$) are less successful in solving the secondary flow cells and predicting the details of the secondary flow contrary to a more sophisticated method like a Detached Eddy Simulation recently used for the simulation of a carrier phase [15].

RNG k-ε model
 1E-06 3.4E-05 6.7E-05 0.0001 $k\text{ (m}^2/\text{s}^2)$

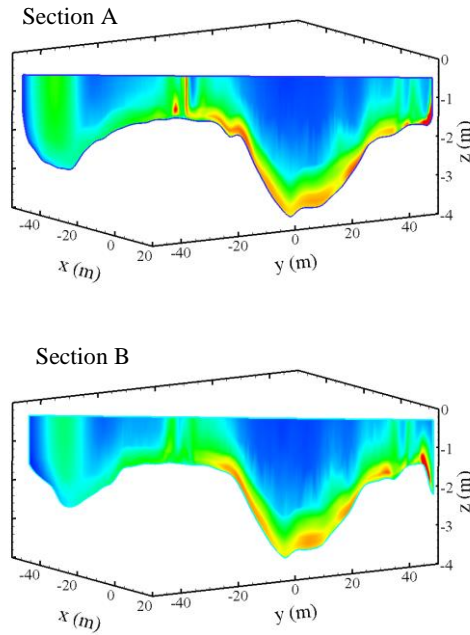


Figure 4 Turbulent kinetic energy (k at cross sections A and B for $RNG\ k-\epsilon$ model (sections from Figure 2).

According to the numerical simulations, it is difficult to make a choice about the turbulence model. We present the results of particle deposition using two models, therefore.

k-ω SST model
 1E-06 3.4E-05 6.7E-05 0.0001 $k\text{ (m}^2/\text{s}^2)$

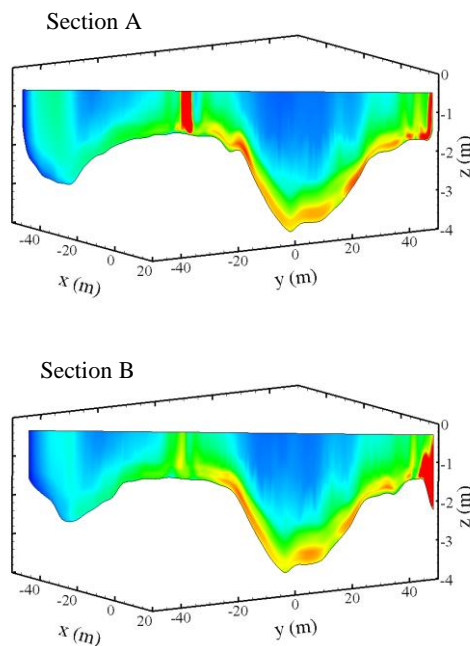


Figure 5 Turbulent kinetic energy at cross sections A and B for $k-\omega\ SST$ model (sections from Figure 2).

4.3. Particles deposition at confluence bed

The spatial distribution of particles deposition taking the particle/turbulence interaction and gravity effect (on the bed confluence) into account is shown in Fig 6. It is seen that the spatial distribution of particles on the bed confluence does not present a significant difference whatever the models used, when particle/turbulence interactions and gravity effect are present. However, if one of the two is absent, the deposition rate or the spatial distribution of particles are greatly affected (Fig. 6 – c and d). In the case when none of them is present, only 1.3 % and 0.9 % of particles are deposited for *RNG k-ε* model and *k-ω SST* model, respectively (see Fig. 7). Indeed, the value of deposition rate is about the same when both gravity effect and particle/turbulence interactions are taken or not into account. (Fig. 7). Moreover, as observed in Ref. [30], the formation of stagnation zone at the upstream of the junction corner of the confluence (Fig. 2 and Fig. 3) causes a sediment transfer between ER and post confluence near the downstream corner, which creates inhomogeneous deposition in bed confluence (Fig. 6 – a and b). In addition, a deposit trend is observed in the deepest part of the confluence and some of the highest levels of *k* (see Sections A and B). Some corridors (dashed black lines in Fig. 6) seem to appear. Whatever the results of particle deposition, it is interesting to note that no deposition occurs near the stagnation zone (at the edge of the junction), although this area is characterized by low fluid velocity values. A possible explanation is that a bar deposit (Fig. 1) is already present in this part of confluence.

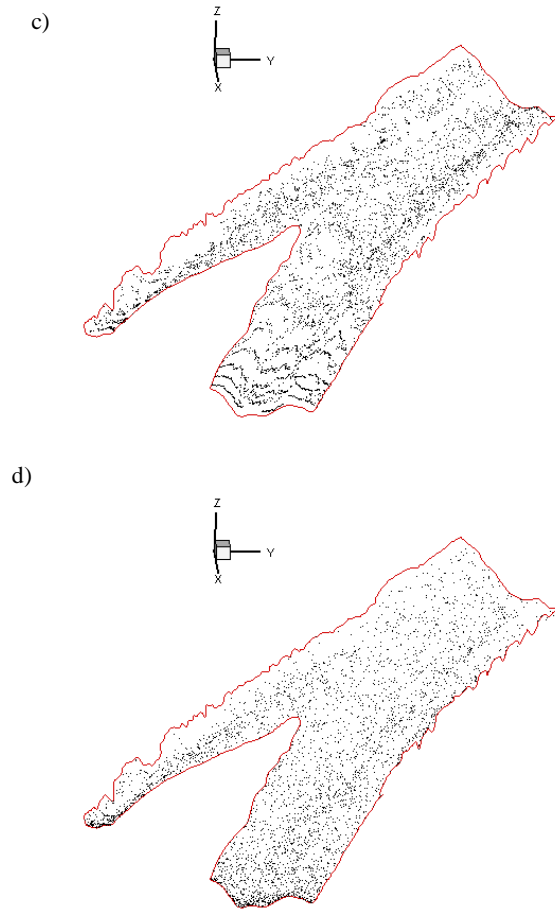
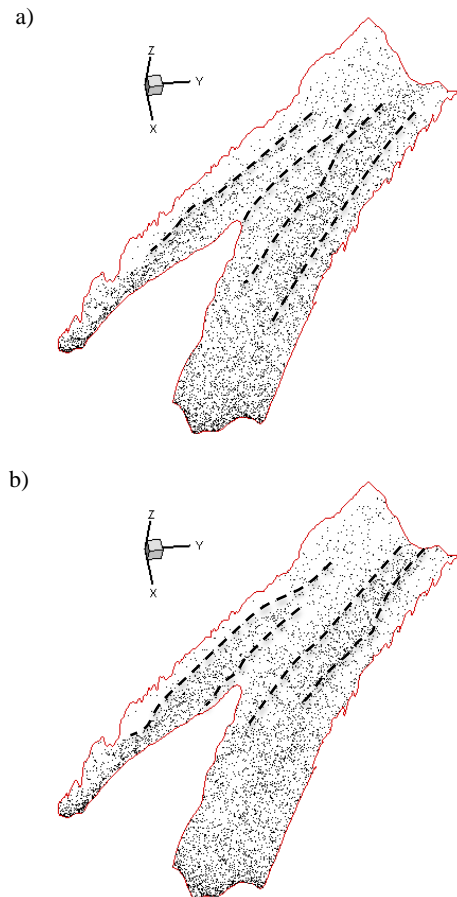


Figure 6 Spatial distribution of particle deposition : a-b) with both EIM and gravity; a) *RNG k-ε* model; b) *k-ω SST* model, c) *RNG k-ε* without EIM; d) *RNG k-ε* without gravity.

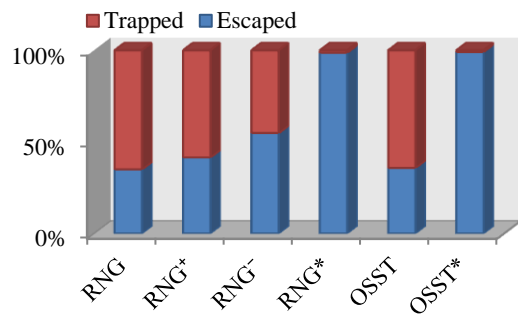


Figure 7 Particles deposition rate : + RNG without EIM, -RNG without gravity and * cases without gravity and EIM.

5. Conclusion

In this paper, sediment deposition within a symmetrical confluence is investigated using an Eulerian/Lagrangian approach (RANS method coupled with a particle Lagrangian tracking) under the influence of the gravity and turbulence. Two turbulence models have been tested (*RNG k-ε* and *k-ω SST* turbulence models). Results show a well-developed stagnation zone at the upstream of the junction corner whatever the model used. A distortion of the mixing layer appear but values of the

turbulence kinetic energy in this zone are different according to the turbulence model. About the modelling of particle deposition in a natural confluence river, results show that the choice of the turbulence model has no real influence on the deposition results. Besides, particle/turbulence interactions or gravity effects have to be considered in simulations since they can have a strong influence on particle distribution and on deposition rate on the confluence bed. In the present study, the gravity effect combined to particle/turbulence interactions are the main deposition mechanisms.

References

- [1] E. H. Taylor, "Flow characteristics at rectangular open-channel junctions," *Transactions, ASCE*, vol. 109, no. 893-912, 1944.
- [2] N. B. Webber and C. A. Greated, "An investigation of flow behaviour at the junction of rectangular channel," *Proceedings of the Institution of Civil Engineers*, pp. 321-344, 1966.
- [3] P. Biron, J. L. Best and A. G. Roy, "Effects of bed discordance on flow dynamics at open channel confluences," *Journal of Hydraulic Engineering*, vol. 122, pp. 676-682, 1996.
- [4] R. B. Bryan and N. J. Kuhn, "Hydraulic conditions in experimental rill confluences and scour in erodible soils," *Water Resources Research*, vol. 38, 2002.
- [5] L. Schindfessel, S. Creëlle and T. D. Mulder, "Flow patterns in an open channel confluence with increasingly dominant tributary inflow," *Water*, 2015.
- [6] M. P. Mosley, "An experimental study of channel confluences," *Journal of Geology*, vol. Vol.84, pp. p.535-562, 1976.
- [7] J. L. Best, "Sediment transport and bed morphology at river channel confluences," *Sedimentology*, vol. 35, pp. 481-498, 1988.
- [8] S. Guillen-Ludena, M. J. Franca, A. H. Cardoso and A. J. Schleiss, "Hydro-morphodynamic evolution in a 90° movable bed discordant confluence with low discharge ratio," *Earth Surface Processes and Landforms*, 2015.
- [9] P. Biron, A. G. Roy, J. L. Best and C. I. Boyer, "Bed morphology and sedimentology at the confluence of unequal depth channels, measurement," *Geomorphology*, vol. 8, pp. 115-129, 1993.
- [10] B. De Serres, A. G. Roy, P. M. Biron and J. L. Best, "Three-dimensional structure of flow at a confluence of river channels with discordant beds," *Geomorphology*, vol. 26, pp. 313-335, 1999.
- [11] J. D. Riley, B. L. Rhoads, D. R. Parsons and K. K. Johnson, "Influence of junction angle on threedimensional flow structure and bed morphology at confluent meander bends during different hydrological conditions," *Earth Surface Process and Landforms*, 2014.
- [12] M. P. Biron, A. S. Ramamurthy and S. Han, "Three-dimensional numerical modeling of mixing at river confluences," *Journal of Hydraulic Engineering*, vol. 130, pp. 243-253, 2004.
- [13] K. F. Bradbrook, S. N. Lane and K. S. Richards, "Numerical simulation of three-dimensional, time-averaged flow structure at river channel confluences," *Journal of Water Resources Research*, vol. 36, pp. 2731-2746, 2000.
- [14] K. F. Bradbrook, S. N. Lane, K. S. Richards, P. M. Biron and A. G. Roy, "Large Eddy Simulation of periodic flow characteristics at river channel confluences," *Journal of Hydraulic Research*, 2000.
- [15] G. Constantinescu, S. Miyawaki, B. Rhoads, A. Sukhodolov and A. G. Kirkil, "Structure of turbulent flow at a river confluence with a momentum ratio close to one: insight provided by an eddy-resolving simulation," *Water Resources Research*, vol. 47, 2011.
- [16] F. Hjulstrom, "Studies of the morphological activity of rivers as illustrated by the River F," *Bulletin of the Geological Institute University of Uppsala*, vol. 25, pp. 221-527, 1935.
- [17] A. Shields, "Application of similarity principles and turbulence research to bed-load movement," *Hydrodynamics Laboratory Publication*, vol. 167, 1936.
- [18] L. C. VanRijn, "Principles of sediment transport in rivers, estuaries and coastal seas. Part I, Aqua, 1993.
- [19] A. Radice, S. Malavasi and F. Ballio, "Solid transport measurements through image processing," *Experiments in Fluids*, vol. 41, pp. 721-734, 2006.
- [20] A. Li and G. Ahmadi, "Dispersion and deposition of spherical particles from point sources in a Turbulent channel flow," *Aerosol Science and Technology*, vol. 16, pp. 209-226, 1992.
- [21] M. Shams, G. Ahmadi and D. H. Smith, "Computational modeling of flow and sediment transport and deposition in meandering rivers," *Advances in Water Resources*, vol. 25, pp. 689-699, 2002.
- [22] A. Fluent, "Theory Guide," 2013.
- [23] V. Yakhot and S. A. Orszag, "Renormalization Group Analysis of Turbulence. I. Basic Theory," *Journal of Scientific Computing*, vol. 1, pp. 3-51, 1986.
- [24] F. R. Menter, "Two-equation eddy-viscosity turbulence models for engineering applications," *AIAA Journal*, vol. 32, pp. 1598-1605, 1994.
- [25] S. A. Morsi and A. J. Alexander, "An investigation of particle trajectories in twophase flow systems," *Journal of Fluid Mechanics*, vol. 55, pp. 193-208, 1972.
- [26] A. D. Gosman and E. Ioannides, "Aspects of computer simulation of liquid-fueled combustors," *Journal Energy*, vol. 7, pp. 482-490, 1983.
- [27] J. R. Cash and A. H. Karp, "A variable order Runge-Kutta method for initial value problems with rapidly varying right-hand sides," *ACM Transactions on Mathematical Software*, vol. 16, pp. 201-222, 1990.
- [28] J. L. Best and A. G. Roy, "Mixing-layer distortion at the confluence of different depth," *Letters to Nature*, vol. 350, pp. 411-413, 1991.
- [29] J. L. Best, "The morphology of river channel confluences," *Progress in Physical Geography*, vol. 10, pp. 157-174, 1986.
- [30] M. L. Ribeiro, K. Blanckaert, A. G. Roy and A. J. Schleiss, "Flow and sediment dynamics in channel confluences," *Journal of Geophysical Research*, vol. 117, 2012.